

# An efficient method for computing stationary states of phase field crystal models

Kai Jiang, Wei Si

*School of Mathematics and Computational Science, Xiangtan University, Xiangtan, Hunan, P.R. China, 411105.*

Chenglong Bao\*

*Yau Mathematical Sciences Center, Tsinghua University, Beijing, P. R. China, 100084.*

## Abstract

Computing stationary states is an important topic for phase field crystal (PFC) models. Great efforts have been made for energy dissipation of the numerical schemes when using gradient flows. However, it is always time-consuming due to the requirement of small effective time steps. In this paper, we propose an adaptive accelerated proximal gradient method for finding the stationary states of PFC models. The energy dissipation is guaranteed and the convergence property is established for the discretized energy functional. Moreover, the connections between generalized proximal operator with classical (semi-)implicit and explicit schemes for gradient flow are given. Extensive numerical experiments, including two three dimensional periodic crystals in Landau-Brazovskii (LB) model and a two dimensional quasicrystal in Lifshitz-Petrich (LP) model, demonstrate that our approach has adaptive time steps which lead to significant acceleration over semi-implicit methods for computing complex structures. Furthermore, our result reveals a deep physical mechanism of the simple LB model via which the sigma phase is first discovered.

**Keywords** Phase field crystal models, Stationary states, Spectral collocation method, Semi-implicit scheme, Adaptive time step

**AMS subject classifications** 35J60, 35Q74, 65N35

**DOI**

## 1. Introduction

The phase field crystal (PFC) model is an important approach to describe many physical processes and material properties, such as the formation of ordered structures, nucleation process, crystal growth, elastic and plastic deformations of the lattice, dislocations, etc [8, 21]. More concretely, let the order parameter function be  $\phi(\mathbf{r})$ , the PFC model can be expressed by a free energy functional:

$$E[\phi(\mathbf{r}); \Theta] = G[\phi(\mathbf{r}); \Theta] + F[\phi(\mathbf{r}); \Theta], \quad (1)$$

where  $\Theta$  are the physical parameters,  $F[\phi]$  is the interaction energy with polynomial type or log-type formulation and  $G[\phi]$  is the bulk energy that contains higher-order linear operators to form ordered structures [7, 17, 25]. A typical interaction potential function for a bounded domain  $\Omega$  is

$$G[\phi] = \frac{1}{|\Omega|} \int_{\Omega} \left[ \prod_{j=1}^m (\Delta + q_j^2) \phi \right]^2 d\mathbf{r}, \quad m \in \mathbb{N}$$

which can be used to describe the pattern formation of periodic crystals, quasicrystals and multi-polynary crystals.

\*Corresponding author. Email: clbao@mail.tsinghua.edu.cn

In order to understand the theory of PFC models as well as predict and guide experiments, it requires to find stationary states  $\phi_s(\mathbf{r}; \Theta)$  and construct phase diagrams of the energy functional (1). Mathematically, denote  $V$  to be a feasible space, one should solve the minimization problem

$$\min_{\phi \in V} E[\phi(\mathbf{r}); \Theta], \quad (2)$$

with different physical parameters  $\Theta$ , which brings the tremendous computational burden. Therefore, within appropriate spatial discretization, the goal of this paper is to develop an efficient and robust numerical method for solving (2) with guaranteed convergence.

Most existing numerical methods for computing the stationary states of PFC model can be classified into two categories. The first class of numerical methods solves the steady nonlinear Euler-Lagrange equations of (2) through different spatial discretization approaches. The second class of numerical methods has been designed via the formulation of nonlinear gradient flow equations. In these numerical PDE approaches, the time-dependent nonlinear gradient flows are discretized in space via different numerical methods. In these time discretized approaches, great efforts have been made to keep the energy dissipation which is crucial for convergence. Typical energy stable schemes to the gradient flows include convex splitting and stabilized factor methods, and recently developed invariant energy quadrature, and scalar auxiliary variable approaches for a modified energy [22]. It is noted that the gradient flow approach is able to describe the quasi-equilibrium behavior of PFC systems. Numerically, the gradient flow is discretized in both space and time domain via different discretization techniques and the stationary state is obtained with a proper choice of initial data.

Under an appropriate spatial discretization scheme, the infinite dimensional problem (2) can be formulated as a minimization problem over a finite dimensional space. Thus, there may exist alternative numerical methods that can converge to the steady states quickly by using modern optimization techniques. Similar ideas have been shown success in computing steady states of the Bose-Einstein condensate [28] and the calculation of density functional theory [27, 18]. In the PFC models, the discretized energy is nonlinear and non-convex which consists of two parts: bulk energy and interaction energy. Motivated by the semi-implicit scheme and the accelerated proximal gradient (APG) method [5, 26] which has been successfully applied in image processing and machine learning, we propose an efficient numerical method for calculating the steady states of (2). As the traditional APG method is proposed for convex problem and its oscillation phenomenon slows down the convergence [20, 24], the restart scheme has been used for accelerating the convergence. Moreover, the numerical speed can be further accelerated by using the line search starting with Barzilai-Borwein steps [2]. The connection of classical explicit/implicit schemes in gradient flows and proximal gradient methods is also built by defining a generalized proximal operator. Extensive numerical experiments have demonstrated that our approach can quickly reach the vicinity of an optimal solution with moderately accuracy, even for very challenge cases. As a byproduct, our numerical result reveals a deep physical intension of a simple PFC model, the Landau-Brazovskii (LB) model, by obtaining the sigma phase.

The rest of this paper is organized as follows. Different discretizations of the energy functional via the Fourier pseudospectral approach and the projection method are introduced in section 3. In section 4, we present the gradient type method and the adaptive APG method for solving the discretized minimization problem. The connection between our proposed approach and some existing time discretized schemes in these numerical methods for solving gradient-flow equations has been built in section 5. Numerical results are reported in section 6 to illustrate the efficiency and accuracy of our algorithms. Finally, some concluding remarks are given in section 7.

## 2. Physical models

Two classes of PFC models are considered in the paper. The first one is the Landau-Brazovskii (LB) model which describes periodic structures [7]. The LB model was introduced to investigate the character of phases and phase transition of periodic crystals. It has been discovered in many different scientific fields, e.g., polymeric materials [23]. In particular, the energy functional of LB model is

$$E_{LB}[\phi(\mathbf{r})] = \frac{1}{|\Omega|} \int_{\Omega} \left\{ \frac{\xi^2}{2} [(\Delta + 1)\phi]^2 + \frac{\tau}{2!} \phi^2 - \frac{\gamma}{3!} \phi^3 + \frac{1}{4!} \phi^4 \right\} d\mathbf{r}, \quad (3)$$

where  $\phi(\mathbf{r})$  is a real-valued function which measures the order of system in terms of order parameter.  $\Omega$  is the system volume,  $\xi$  is the bare correlation length,  $\tau$  is the dimensionless reduced temperature,  $\gamma$  is phenomenological coefficient. Compared with double-well bulk energy, the cubic term in the LB functional helps us study the first-order phase transition.

The second one is the Lifshitz-Petrich (LP) model that can simulate quasiperiodic structures, such as the bi-frequency excited Faraday wave [17], and the explanation of the stability of soft-matter quasicrystals [16, 11].

Before we present the LP model, an introduction of the average spacial integral, so-called almost periodic integral, is necessary. For a space-filling structure, such as the quasicrystal, the average spacial integral can be defined as

$$\oint = \lim_{R \rightarrow \infty} \frac{1}{|B_R|} \int_{B_R}, \quad (4)$$

where  $B_R \subset \mathbb{R}^d$  is the ball centred at origin with radii  $R$ . Using the above notation, the energy functional of LP model is given by

$$E_{LP}[\phi(\mathbf{r})] = \oint \left\{ \frac{c}{2} [(\Delta + q_1^2)(\Delta + q_2^2)\phi]^2 + \frac{\varepsilon}{2} \phi^2 - \frac{\kappa}{3} \phi^3 + \frac{1}{4} \phi^4 \right\} d\mathbf{r}, \quad (5)$$

$c$  is the energy penalty,  $\varepsilon$  and  $\kappa$  are phenomenological coefficients.

Formally, the difference between the LB and LP energy functional is the number of length-scale governed by the differential term. The LB model has a one-length-scale which can be used to study the phase behavior of periodic structures [7, 31], while the LP model possesses a two-length-scale that can be used to studied the formation and stability of quasicrystals [17, 16, 11, 9].

### 3. Discretization of the energy functional

In this section, we introduce different discretization schemes of the energy functionals (3) and (5), and reduce them to finite dimensional minimization problems. Two classes of stationary states are considered. The first class of stationary states is periodic in LB model which can be described in a bounded domain. Thus we can truncate the energy functional from the whole space  $\mathbb{R}^d$  to a bounded domain  $\Omega$  with periodic boundary condition. Then we employ Fourier pseudospectral method to discretize LB energy functional. The second class of stationary phases can be quasicrystals in LP model. For these structures, the discretization of the energy functional in a bounded domain results in a significant Diophantine approximation error. In this paper, we apply with the projection method [13], a high dimensional interpretation approach, to discretize the LP energy function (5), which can avoid the Diophantine approximation error.

#### 3.1. Fourier pseudospectral discretization

Each of the  $d$ -dimensional periodic system can be described by a Bravis lattice

$$\mathcal{R} = \sum_{j=1}^d \ell_j \mathbf{a}_j, \quad \ell_j \in \mathbb{Z},$$

where the vector  $\mathbf{a}_j \in \mathbb{R}^d$  forms the primitive Bravis lattice  $\mathbf{A} = (\mathbf{a}_1, \mathbf{a}_2, \dots, \mathbf{a}_d) \in \mathbb{R}^{d \times d}$ . The smallest possible periodicity, or named the unit cell, of the system is

$$\Omega = \sum_{j=1}^d \zeta_j \mathbf{a}_j, \quad \zeta_j \in [0, 1).$$

The associated reciprocal lattice is

$$\mathcal{R}^* = \sum_{j=1}^d h_j \mathbf{b}_j, \quad h_j \in \mathbb{Z}.$$

The primitive reciprocal lattice vector  $\mathbf{b}_j \in \mathbb{R}^d$  satisfies the dual relationship

$$\mathbf{a}_i \mathbf{b}_j = 2\pi \delta_{ij}.$$

Then the periodic function on the Bravis lattice, i.e.,  $\phi(\mathbf{r}) = \phi(\mathbf{r} + \mathcal{R})$ , can be expanded as

$$\phi(\mathbf{r}) = \sum_{\mathbf{h} \in \mathbb{Z}^d} \hat{\phi}(\mathbf{h}) e^{i(\mathbf{B}\mathbf{h})^T \mathbf{r}}, \quad \mathbf{r} \in \Omega,$$

where  $\mathbf{h} = (h_1, h_2, \dots, h_d)^T$ ,  $\mathbf{B} = (\mathbf{b}_1, \mathbf{b}_2, \dots, \mathbf{b}_d) \in \mathbb{R}^{d \times d}$  is invertible. The coefficient,  $\hat{\phi}(\mathbf{h}) = (1/|\Omega|) \int_{\Omega} \phi(\mathbf{r}) e^{-i(\mathbf{B}\mathbf{h})^T \mathbf{r}} d\mathbf{r}$ , satisfies

$$X := \left\{ \{\hat{\phi}(\mathbf{h})\}_{\mathbf{h} \in \mathbb{Z}^d} : \hat{\phi}(\mathbf{h}) \in \mathbb{C}, \sum_{\mathbf{h} \in \mathbb{Z}^d} |\hat{\phi}(\mathbf{h})| < \infty \right\}.$$

In numerical computations, we need to minimize the LB energy functional (3) in a finite dimensional subspace. More precisely, let  $N = (N_1 + 1, N_2 + 1, \dots, N_d + 1) \in \mathbb{N}^d$ , and

$$X_N := \{\hat{\phi}(\mathbf{h}) \in X : \hat{\phi}(\mathbf{h}) = 0, \text{ for all } |\mathbf{h}_j| > N_j/2, j = 1, 2, \dots, d\}.$$

The number of elements in the set is  $N = (N_1 + 1)(N_2 + 1) \cdots (N_d + 1)$ . The order parameter can be projected into the finite dimensional space  $X_N$ , i.e.,

$$\phi(\mathbf{r}) \approx \sum_{\hat{\phi}(\mathbf{h}) \in X_N} \hat{\phi}(\mathbf{h}) e^{i(\mathbf{B}\mathbf{h})^T \mathbf{r}}, \quad \mathbf{r} \in \Omega.$$

Due to the orthonormal condition

$$\frac{1}{|\Omega|} \int_{\Omega} e^{i(\mathbf{B}\mathbf{h}_1)^T \mathbf{r}} e^{-i(\mathbf{B}\mathbf{h}_2)^T \mathbf{r}} d\mathbf{r} = \delta_{\mathbf{h}_1 \mathbf{h}_2},$$

the LB energy functional  $E_{LB}$  can be approximated as

$$\begin{aligned} E_h[\hat{\Phi}] &= \frac{\xi^2}{2} \sum_{\mathbf{h}_1 + \mathbf{h}_2 = \mathbf{0}} [1 - (\mathbf{B}\mathbf{h}_1)^T (\mathbf{B}\mathbf{h}_2)]^2 \hat{\phi}(\mathbf{h}_1) \hat{\phi}(\mathbf{h}_2) + \frac{\tau}{2!} \sum_{\mathbf{h}_1 + \mathbf{h}_2 = \mathbf{0}} \hat{\phi}(\mathbf{h}_1) \hat{\phi}(\mathbf{h}_2) \\ &\quad - \frac{\gamma}{3!} \sum_{\mathbf{h}_1 + \mathbf{h}_2 + \mathbf{h}_3 = \mathbf{0}} \hat{\phi}(\mathbf{h}_1) \hat{\phi}(\mathbf{h}_2) \hat{\phi}(\mathbf{h}_3) + \frac{1}{4!} \sum_{\mathbf{h}_1 + \mathbf{h}_2 + \mathbf{h}_3 + \mathbf{h}_4 = \mathbf{0}} \hat{\phi}(\mathbf{h}_1) \hat{\phi}(\mathbf{h}_2) \hat{\phi}(\mathbf{h}_3) \hat{\phi}(\mathbf{h}_4) \end{aligned}$$

where  $\mathbf{h}_j \in \mathbb{Z}^d$ , Fourier coefficient  $\hat{\phi}(\mathbf{h}) \in X_N$ , and  $\hat{\Phi} = (\hat{\phi}_1, \dots, \hat{\phi}_N)^T \in \mathbb{C}^N$ . The convolutions in the above expression can be calculated by Fourier pseudospectral method through the fast Fourier transform (FFT). Therefore, it reduces to a finite dimensional minimization problem:

$$\min_{\hat{\Phi} \in \mathbb{C}^N} E_h[\hat{\Phi}] = G_h[\hat{\Phi}] + F_h[\hat{\Phi}] \quad (6)$$

where  $G_h$  and  $F_h$  are the discretized interaction and bulk energy, respectively. The gradient of  $E_h[\hat{\Phi}]$  is

$$\nabla E_h[\hat{\Phi}] = \xi^2 \Lambda \hat{\Phi} + \tau \hat{\Phi} - \frac{\gamma}{2} \mathcal{F}_N^{-1}((\mathcal{F}_N \hat{\Phi})^2) + \frac{1}{6} \mathcal{F}_N^{-1}((\mathcal{F}_N \hat{\Phi})^3)$$

where  $\Lambda \in \mathbb{C}^{N \times N}$  is a diagonal matrix with entries  $[1 - (\mathbf{B}\mathbf{h})^T (\mathbf{B}\mathbf{h})]^2$  and  $\mathcal{F}_N \in \mathbb{C}^{N \times N}$  is the discretized Fourier transform matrix.

### 3.2. Projection method discretization

For the  $d$ -dimensional quasicrystals which are the space-filling structures, the spatial integral  $\frac{1}{|\Omega|} \int_{\Omega}$  in the energy functional (1) shall be instead by the almost periodic spacial integral  $\oint$ , as defined by Eq. (4). We immediately have the following orthonormal property:

$$\oint e^{i\mathbf{k} \cdot \mathbf{r}} e^{-i\mathbf{k}' \cdot \mathbf{r}} d\mathbf{r} = \delta_{\mathbf{k}\mathbf{k}'}, \quad \forall \mathbf{k}, \mathbf{k}' \in \mathbb{R}^d. \quad (7)$$

For an almost periodic function, the average transformation is

$$\hat{\phi}(\mathbf{k}) = \oint \phi(\mathbf{r}) e^{-i\mathbf{k} \cdot \mathbf{r}} d\mathbf{r}, \quad \mathbf{k} \in \mathbb{R}^d,$$

and it is well defined [14]. In this paper, we carry out the above computation in a higher dimension using the projection method which is based on the fact that a  $d$ -dimensional quasicrystal can be embedded into an  $n$ -dimensional periodic structure ( $n \geq d$ ) [10]. Using the projection method, the order parameter  $\phi(\mathbf{r})$  is

$$\phi(\mathbf{r}) = \sum_{\mathbf{h} \in \mathbb{Z}^n} \hat{\phi}(\mathbf{h}) e^{i[(\mathcal{P}\mathbf{B}\mathbf{h})^T \cdot \mathbf{r}]}, \quad \mathbf{r} \in \mathbb{R}^d, \quad (8)$$

where  $\mathbf{B} \in \mathbb{R}^{n \times n}$  is invertible, related to the  $n$ -dimensional primitive reciprocal lattice and the projection matrix  $\mathcal{P} \in \mathbb{R}^{d \times n}$  depends on the property of quasicrystals, such as rotational symmetry [10]. The Fourier coefficient  $\hat{\phi}(\mathbf{h})$  satisfies

$$X := \left\{ (\hat{\phi}(\mathbf{h}))_{\mathbf{h} \in \mathbb{Z}^n} : \hat{\phi}(\mathbf{h}) \in \mathbb{C}, \sum_{\mathbf{h} \in \mathbb{Z}^n} |\hat{\phi}(\mathbf{h})| < \infty \right\}.$$

Again, in practice, we need to minimize the LP energy functional (3) in a finite dimensional subspace. More precisely, let  $N = (N_1, N_2, \dots, N_n) \in \mathbb{N}^n$ , and

$$X_N := \{\hat{\phi}(\mathbf{h}) \in X : \hat{\phi}(\mathbf{h}) = 0, \text{ for all } |\mathbf{h}_j| > N_j/2, j = 1, 2, \dots, n\}.$$

The number of elements in the set is  $N = (N_1 + 1)(N_2 + 1) \cdots (N_n + 1)$ . Together with (7) and (8), the discretized energy function (5) is

$$\begin{aligned} E_h[\hat{\Phi}] = & \frac{c}{2} \sum_{\mathbf{h}_1 + \mathbf{h}_2 = \mathbf{0}} \left[ q_1^2 - (\mathcal{P}\mathbf{B}\mathbf{h})^T (\mathcal{P}\mathbf{B}\mathbf{h}) \right]^2 \left[ q_2^2 - (\mathcal{P}\mathbf{B}\mathbf{h})^T (\mathcal{P}\mathbf{B}\mathbf{h}) \right]^2 \hat{\phi}(\mathbf{h}_1) \hat{\phi}(\mathbf{h}_2) \\ & + \frac{\varepsilon}{2} \sum_{\mathbf{h}_1 + \mathbf{h}_2 = \mathbf{0}} \hat{\phi}(\mathbf{h}_1) \hat{\phi}(\mathbf{h}_2) - \frac{\kappa}{3} \sum_{\mathbf{h}_1 + \mathbf{h}_2 + \mathbf{h}_3 = \mathbf{0}} \hat{\phi}(\mathbf{h}_1) \hat{\phi}(\mathbf{h}_2) \hat{\phi}(\mathbf{h}_3) \\ & + \frac{1}{4} \sum_{\mathbf{h}_1 + \mathbf{h}_2 + \mathbf{h}_3 + \mathbf{h}_4 = \mathbf{0}} \hat{\phi}(\mathbf{h}_1) \hat{\phi}(\mathbf{h}_2) \hat{\phi}(\mathbf{h}_3) \hat{\phi}(\mathbf{h}_4), \end{aligned} \quad (9)$$

where  $\mathbf{h}_j \in \mathbb{Z}^n$ ,  $\hat{\phi}_j \in X_N$ ,  $j = 1, 2, \dots, 4$ ,  $\hat{\Phi} = (\hat{\phi}_1, \hat{\phi}_2, \dots, \hat{\phi}_N) \in \mathbb{C}^N$ . It is clear that the nonlinear (quadratic, cubic and cross) terms in Eq. (9) are  $n$ -dimensional convolutions in the reciprocal space. A direct evaluation of these convolution terms is extremely expensive. Instead, these terms are simple multiplication in the  $n$ -dimensional real space. Again, the efficient pseudospectral approach is applied to calculate these convolutions in Eq. (9) through the  $n$ -dimensional FFT.

Therefore, it leads to the following finite dimensional minimization problem:

$$\min_{\hat{\Phi} \in \mathbb{C}^N} E_h[\hat{\Phi}] = G_h[\hat{\Phi}] + F_h[\hat{\Phi}],$$

where  $G_h$  and  $F_h$  are the discretized interaction and bulk energies. The gradient of  $E_h[\hat{\Phi}]$  is

$$\nabla E_h[\hat{\Phi}] = \xi^2 \Lambda \hat{\Phi} + \tau \hat{\Phi} - \frac{\gamma}{2} \mathcal{F}_N^{-1}((\mathcal{F}_N \hat{\Phi})^2) + \frac{1}{6} \mathcal{F}_N^{-1}((\mathcal{F}_N \hat{\Phi})^3)$$

where  $\Lambda \in \mathbb{C}^{N \times N}$  is a diagonal matrix with entries  $[q_1^2 - (\mathcal{P}\mathbf{B}\mathbf{h})^T (\mathcal{P}\mathbf{B}\mathbf{h})]^2 [q_2^2 - (\mathcal{P}\mathbf{B}\mathbf{h})^T (\mathcal{P}\mathbf{B}\mathbf{h})]^2$ . The  $\mathcal{F}_N \in \mathbb{C}^{N \times N}$  is the discretized Fourier transform matrix and  $\mathcal{F}_N^{-1}$  is the corresponding inverse discretized Fourier transform matrix. In the following, we will neglect the superscript of hat for simplicity.

#### 4. The proposed numerical approach

In this section, we first review the classical semi-implicit method and accelerated proximal gradient (APG) method and then propose the adaptive APG method with proved convergence. Finally, the connection of generalized proximal operator with gradient flows approaches is present.

##### 4.1. Semi-implicit scheme

The semi-implicit scheme is a simple but useful approach for finding the stationary state based on gradient flows. For example, the Allen-Cahn equation of the discretized energy functional is

$$\Phi_t = -\nabla G_h[\Phi] - \nabla F_h[\Phi]$$

with the periodic condition and  $t$  is the spurious time variable. Given an initial value  $\Phi_0$  and the time step  $\alpha$ , the semi-implicit scheme is

$$\frac{1}{\alpha}(\Phi_{k+1} - \Phi_k) = -\nabla G_h[\Phi_{k+1}] - \nabla F_h[\Phi_k], \quad (10)$$

where  $\Phi_k$  is the approximation of the solution at  $k\alpha$ , i.e.,  $\Phi(k\alpha)$ . The semi-implicit scheme satisfies the following energy dissipation property.

**Theorem 4.1.** *Let  $E_h[\Phi] = F_h[\Phi] + G_h[\Phi]$ . Assume that there exists a constant  $L > 0$  such that the bulk energy  $F_h[\Phi]$  satisfies  $\max_{\Phi \in \mathbb{C}^N} \|\nabla^2 F_h[\Phi]\|_2 \leq L$ , and the time step length  $\alpha \leq 1/L$ , then the solutions of (10) satisfy*

$$E_h[\Phi_{k+1}] \leq E_h[\Phi_k], \quad \forall k \geq 0.$$

*Proof.* From (10), it is easy to know

$$\Phi_{k+1} \in \operatorname{argmin}_{\Phi} F_h[\Phi_k] + \langle \nabla F_h[\Phi_k], \Phi - \Phi_k \rangle + \frac{1}{2\alpha} \|\Phi - \Phi_k\|^2 + G_h[\Phi].$$

It implies

$$\begin{aligned} F_h[\Phi_k] + G_h[\Phi_k] &\geq F_h[\Phi_k] + \langle \nabla F_h[\Phi_k], \Phi_{k+1} - \Phi_k \rangle + \frac{1}{2\alpha} \|\Phi_{k+1} - \Phi_k\|^2 + G_h[\Phi_{k+1}] \\ &\geq F_h[\Phi_{k+1}] + G_h[\Phi_{k+1}] + \left( \frac{1}{2\alpha} - \frac{L}{2} \right) \|\Phi_{k+1} - \Phi_k\|^2, \end{aligned}$$

where the last inequality is from the Taylor expansion of  $F_h$  and the boundedness constraint on  $\nabla^2 F_h$ .  $\square$

Therefore, to satisfy the energy dissipation law, the time step length  $\alpha$  depends on the Lipschitz constant  $L$ . In a general PFC model, the universal Lipschitz constant  $L$  may not exist or be very large in bounded domain which leads to a small time step and slows down the convergence speed. Despite its strict requirements on  $\alpha$  in theory, the semi-implicit scheme works well in practice which inspires us a further exploration of the semi-implicit scheme. In the following context, we will combine modern optimization approaches and the semi-implicit scheme to obtain a more efficient approach.

#### 4.2. Accelerated proximal gradient (APG) method

The classical APG method [5, 26] is designed for solving the convex composite problem:

$$\min_{x \in \mathbb{H}} H(x) = g(x) + f(x) \quad (11)$$

where  $\mathbb{H}$  is the finite dimensional Hilbert space equipped with the inner product  $\langle \cdot, \cdot \rangle$ ,  $g$  and  $f$  are both continuously convex and  $\nabla f$  has a Lipschitz constant  $L$ , i.e.

$$\|\nabla f(x) - \nabla f(y)\| \leq L\|x - y\|, \quad \forall x, y \in \mathbb{H}.$$

Given initializations  $x_1 = x_0$  and  $t_0 = 1$ , the APG method consists of the following steps:

$$t_k = (\sqrt{4(t_{k-1})^2 + 1} + 1)/2, \quad (12a)$$

$$\begin{aligned} y_k &= x_k + \frac{t_{k-1} - 1}{t_k} (x_k - x_{k-1}), \\ x_{k+1} &= \operatorname{Prox}_g^\alpha(y_k - \alpha \nabla f(y_k)), \end{aligned} \quad (12b)$$

where  $\alpha \in (0, 1/L]$  and the mapping  $\operatorname{Prox}_g^\alpha(\cdot) : \mathbb{R}^n \mapsto \mathbb{R}^n$  is defined as

$$\operatorname{Prox}_g^\alpha(x) = \operatorname{argmin}_y \left\{ g(y) + \frac{1}{2\alpha} \|y - x\|^2 \right\}. \quad (13)$$

It is noted that the proximal map in (13) is well defined as  $g$  is convex. Moreover, the step size  $\alpha$  can be set adaptively as long as the following inequality holds:

$$H(x_{k+1}) \leq Q_{\alpha_k}(x_{k+1}, x_k) \leq H(x_k)$$

where

$$Q_\alpha(x, y) = f(y) + \langle x - y, \nabla f(y) \rangle + \frac{1}{2\alpha} \|x - y\|^2 + g(x).$$

The APG method has the attractive convergence property as follows.

**Theorem 4.2** ([5]). *Let  $\{x_k\}, \{y_k\}$  be the sequence generated by the (12a)-(12b) and  $H^*$  be the optimal objective value of (11) and  $X_*$  be the set of minimizers. For any  $k \geq 1$ , we have*

$$H(x_k) - H^* \leq \frac{2\|x_0 - x^*\|^2}{\alpha(k+1)^2}, \quad \forall x^* \in X_*.$$

#### 4.3. Adaptive APG method

The discretized energy functional  $E[\Phi]$  in (6) can be reformulated as form (11) by setting

$$f = F[\Phi] \quad \text{and} \quad g = G[\Phi].$$

We omit the subscript  $h$  for simplicity. However, there are two main obstacles when directly applying APG method for solving phase field models as  $F$  is non-convex and  $\nabla F$  has no universal Lipschitz constant. In this paper, we propose an efficient and convergent numerical algorithm for solving the discretized phase field model (6) by combining APG method with restart techniques.

The restart techniques for the APG method was proposed in [20] which has shown significant acceleration of the APG method by imposing the decreasing property of the objective value when solving convex problems. Furthermore, another restart strategy called speed restart is developed in [24] to ensure the linear convergence of the proposed restart APG method for strongly convex problems. In recent years, the restart techniques have been furtherer applied for solving non-convex composite problems in image processing [3]. We introduce the details of the proposed algorithm in the following context.

Let  $\Phi_k$  and  $\Phi_{k-1}$  be the current and previous states respectively and the extrapolation weight  $w_k = (t_{k-1} - 1)/t_k$ . We can obtain a candidate state by

$$\Psi_{k+1} = \text{Prox}_G^{\alpha_k}(\tilde{\Phi}_k - \alpha_k \nabla F[\tilde{\Phi}_k]), \quad (14)$$

where

$$\tilde{\Phi}_k = \Phi_k + w_k(\Phi_k - \Phi_{k-1}).$$

It is noted that the proximal mapping in (14) is well defined as  $G$  is convex. Different from the APG method, the restart technique is to determine whether we accept the result  $\Psi_{k+1}$  as the new estimate  $\Phi_{k+1}$ . Inspired by the function value restart condition in [20], we choose  $\Phi_{k+1} = \Psi_{k+1}$  whenever the following condition holds:

$$E[\Phi_k] - E[\Psi_{k+1}] \geq \delta \|\Phi_k - \Psi_{k+1}\|^2 \quad (15)$$

for some  $\delta > 0$ . If the condition (15) does not hold, we restart the APG by setting  $w_k = 0$ . In this case, we have

$$\Phi_{k+1} = \text{Prox}_G^{\alpha_k}(\Phi_k - \alpha_k \nabla F(\Phi_k)). \quad (16)$$

In fact, the scheme (16) provides an adaptive time step semi-implicit approach when  $\alpha_k$  varies. From the continuity of  $F, G$  in (6) and the coercive property of  $F$ , i.e.

$$F(\Phi) \rightarrow +\infty, \quad \Phi \rightarrow +\infty,$$

the sub-level set  $\{E \leq E[\Phi_0]\} = \{\Phi \in \mathbb{H} \mid E[\Phi] \leq E[\Phi_0]\}$  is compact for any  $\Phi_0$ . Let  $\mathcal{M}$  be the closed ball that contains  $[E \leq E[\Phi_0]]$ . From the smoothness of  $F$ ,  $\nabla F$  is Lipschitz continuous in  $\mathcal{M}$ . Denote  $L_{\mathcal{M}}$  to be the Lipschitz constant of  $\nabla F$  in the set  $\mathcal{M}$ , i.e.

$$\|\nabla F[\Phi] - \nabla F[\Psi]\| \leq L_{\mathcal{M}} \|\Phi - \Psi\|, \quad \forall \Phi, \Psi \in \mathcal{M}.$$

Thus, we obtain the the next proposition that shows  $\Phi_k \in \mathcal{M}$  satisfying the sufficient decrease condition for all  $k$ .

**Proposition 4.3.** *Given an initial point  $\Phi_0$  and the iterates  $\Phi_{k+1} = \text{Prox}_G^{\alpha_k}(\Phi_k - \alpha_k \nabla F(\Phi_k))$  with  $\alpha_k \in (0, 1/L_{\mathcal{M}})$  for  $k = 0, 1, \dots$ . If  $\{\Phi_k\}_{k=1}^{\infty} \subset \mathcal{M}$ , then*

$$E[\Phi_k] - E[\Phi_{k+1}] \geq (1/2\alpha_k - L_{\mathcal{M}}/2) \|\Phi_{k+1} - \Phi_k\|^2, \quad \forall k = 1, 2, \dots$$

The proof can be easily obtained from Theorem 4.1. Let  $\Phi_{k+1}$  is from (16) and  $\eta \leq \frac{1}{2\alpha_k} - \frac{L_{\mathcal{M}}}{2}$ , the following sufficient condition

$$E[\Phi_k] - E[\Phi_{k+1}] \geq \eta \|\Phi_{k+1} - \Phi_k\|^2 \quad (17)$$

holds and thus the (16) is a safe-guard step which ensures energy dissipation. On the other hand, by Proposition 4.3,  $\alpha_k$  should be less than  $1/L_{\mathcal{M}}$  which might be very small. Thus, it only allows a small step size which may significantly slow down the convergence, and be always too conservative. By line search technique, we can adaptively estimate the step size  $\alpha_k$  which will be introduced as follows.

**Estimation of step size  $\alpha_k$ .** Define:  $s_{k-1} := \Phi_k - \Phi_{k-1}$ , and  $g_{k-1} := \nabla F[\Phi_k] - \nabla F[\Phi_{k-1}]$ . We initialize the search step by the Barzilai-Borwein (BB) method [4], i.e.

$$\beta_0 = \frac{\langle s_{k-1}, s_{k-1} \rangle}{\langle s_{k-1}, g_{k-1} \rangle} \quad \text{or} \quad \beta_0 = \frac{\langle s_{k-1}, g_{k-1} \rangle}{\langle g_{k-1}, g_{k-1} \rangle}. \quad (18)$$

Together with the standard backtracking, we adopt the step size  $\alpha_k$  whenever (17) holds. The detailed algorithm of estimation the step size  $\alpha_k$  is given in Algorithm 1. and the proposed adaptive APG algorithm is present in Algorithm 2.

---

**Algorithm 1** Estimation of  $\alpha_k$  at  $\Psi_k$ 

---

```
1: Inputs:  $\Phi_k, \Psi_k, \nabla F[\Psi_k], \nabla F[\Phi_k], \rho \in (0, 1)$  and  $\eta > 0$ 
2: Output: step size  $\alpha_k$ 
3: Set  $s_k = \Psi_k - \Phi_k$  and  $d_k = \nabla F[\Psi_k] - \nabla F[\Phi_k]$ .
4: Initialize  $\beta$  by the Barzilai-Borwein method via Eqn.(18)
5: for  $j = 1, 2, \dots$  do
6:   Calculate  $\Psi_{k+1} = \text{Prox}_G^\beta(\Psi_k - \beta \nabla F[\Psi_k])$ 
7:   Step size length  $\beta$  is obtained by the linear search technique
8:   if  $E[\Psi_k] - E[\Psi_{k+1}] \geq \eta \|\Psi_k - \Psi_{k+1}\|^2$  then
9:      $\alpha_k = \beta$  and break
10:  else
11:     $\beta = \rho \beta$ 
12:  end if
13: end for
```

---

---

**Algorithm 2** Adaptive APG algorithm for PFC model

---

```
1: Initialize  $\Phi_1 = \Phi_0, w_0 \in [0, 1], N_{max} \in \mathbb{N}, k_{ada} = 0, \eta \geq \delta > 0$ .
2: for  $k = 1, 2, 3, \dots$  do
3:   Update  $w_k \in [0, 1]$ 
4:   Update  $\Psi_k = (1 + w_k)\Phi_k - w_k\Phi_{k-1}$ 
5:   Estimate the step size  $\alpha_k$  at  $\Psi_k$  via Algorithm 1
6:   Calculate  $\Psi_{k+1} = \text{Prox}_G^{\alpha_k}(\Psi_k - \alpha_k \nabla F[\Psi_k])$ .
7:   if  $E[\Phi_k] - E[\Psi_{k+1}] \geq \delta \|\Phi_k - \Psi_{k+1}\|^2$  holds and  $k - k_{ada} \leq N_{max}$  then
8:     Set  $\Phi_{k+1} = \Psi_{k+1}$ .
9:   else
10:    Reset  $w_k = 0$  and  $k_{ada} = k$ .
11:   end if
12: end for
```

---

#### 4.3.1. Convergence analysis

In this section, we show that our proposed method converges to a steady state of the original energy function. Firstly, we present a useful lemma for our analysis.

**Lemma 4.4** (Uniformized Kurdyka-Lojasiewicz property [6]). *Let  $\Omega$  be a compact set and  $E$  defined in (6) be bounded below. Assume that  $E$  is constant on  $\Omega$ . Then, there exist  $\epsilon > 0, \eta > 0$ , and  $\psi \in \Psi_\eta$  such that for all  $\bar{u} \in \Omega$  and all  $u \in \Gamma_\eta(\bar{u}, \epsilon)$ , one has,*

$$\psi'(E(u) - E(\bar{u})) \|\nabla E(u)\| \geq 1,$$

where  $\Psi_\eta = \{\psi \in C[0, \eta) \cap C^1(0, \eta) \text{ and } \psi \text{ is concave, } \psi(0) = 0, \psi' > 0 \text{ on } (0, \eta)\}$  and  $\Gamma_\eta(x, \epsilon) = \{y \mid \|x - y\| \leq \epsilon, E(x) < E(y) < E(x) + \eta\}$ .

*Proof.* The proof is based on the facts that  $F$  and  $G$  satisfy the so called Kurdyka-Lojasiewicz property on  $\Omega$  [6].  $\square$

**Theorem 4.5.** *Let  $E$  defined in (6) be bounded below and  $\{\Phi_k\}$  be the sequence generated by Algorithm 2. If  $\Phi_k \in \mathcal{M}$  and  $\liminf_k \alpha_k = \bar{\alpha} > 0$ , then  $\{\Phi_k\}$  has the global convergence property, i.e. there exists a point  $\Phi^*$  such that  $\nabla E[\Phi^*] = \mathbf{0}$  and  $\lim_{k \rightarrow +\infty} \Phi_k = \Phi^*$ .*

*Proof.* Define

$$P_{k+1} = \text{Prox}_G^{\alpha_k}(\Phi_k - \alpha_k \nabla F[\Phi_k]) \quad (19)$$

and two sets  $\Omega_2 = \{k \mid t_k = 1\}$  and  $\Omega_1 = \mathbb{N} \setminus \Omega_2$ . It is noted that for any  $k \in \Omega_2$ , we have  $\Phi_{k+1} = P_{k+1}$ . Let  $w_k = (t_k - 1)/t_{k+1}$ , then there exists some  $\bar{w} = (t_{N_{max}} - 1)/(t_{N_{max}} + 1) \in [0, 1)$  such that  $w_k \leq \bar{w}$  for all  $k$  as  $t_k$  is increasing and  $t_k$  is reset to 1 at most every  $N_{max}$  iteration. We show the following properties of the sequence  $\{x_k\}$  generated by Algorithm 2.

**Sufficient decrease property.** If  $k \in \Omega_2$ , we have

$$E[\Phi_k] - E[\Phi_{k+1}] \geq \max(1/2\alpha_k - L_{\mathcal{M}}/2, \eta) \|\Phi_k - \Phi_{k+1}\|^2$$

from Proposition 4.3 and the line search criterion (17). Together with the condition (15), the following *sufficient decrease property* holds

$$E[\Phi_k] - E[\Phi_{k+1}] \geq \rho_1 \|\Phi_k - \Phi_{k+1}\|^2, \quad \forall k, \quad (20)$$

where  $\rho_1 = \min\{\eta, \delta\} > 0$ . Since  $\inf E > -\infty$ , there exists  $E^*$  such that  $E[\Phi_k] \geq E^*$  and  $E[\Phi_k] \rightarrow E^*$  as  $k \rightarrow +\infty$ . This implies

$$\rho_1 \sum_{k=0}^{\infty} \|\Phi_{k+1} - \Phi_k\|^2 \leq E[\Phi_0] - E^* < +\infty \text{ and } \lim_{k \rightarrow +\infty} \|\Phi_{k+1} - \Phi_k\| = 0. \quad (21)$$

**Bounded the gradient.** If  $k \in \Omega_1$ , by the optimality condition of (14), we have

$$-\nabla F[\tilde{\Phi}_k] + \frac{1}{\alpha_k}(\tilde{\Phi}_k - \Phi_{k+1}) = \nabla G[\Phi_{k+1}].$$

Thus,  $\nabla F[\Phi_{k+1}] - \nabla F[\tilde{\Phi}_k] + \frac{1}{\alpha_k}(\tilde{\Phi}_k - \Phi_{k+1}) = \nabla E[\Phi_{k+1}]$  and

$$\begin{aligned} \|\nabla E[\Phi_{k+1}]\| &\leq (L_{\mathcal{M}} + 1/\bar{\alpha})\|\Phi_{k+1} - \tilde{\Phi}_k\| \\ &\leq (L_{\mathcal{M}} + 1/\bar{\alpha})(\|\Phi_{k+1} - \Phi_k\| + w_k\|\Phi_k - \Phi_{k-1}\|), \end{aligned} \quad (22)$$

as  $\tilde{\Phi}_k \in \mathcal{M}$  where  $\mathcal{M}$  is a bounded set and  $L_{\mathcal{M}}$  is the Lipschitz constant of  $\nabla F$  in  $\mathcal{M}$ . If  $k \in \Omega_2$ , by the optimality condition of (19), we have

$$-\nabla F[\Phi_k] + \frac{1}{\alpha_k}(\Phi_k - \Phi_{k+1}) = \nabla G[\Phi_{k+1}].$$

Then,  $\nabla F[\Phi_{k+1}] - \nabla F[\Phi_k] + \frac{1}{\alpha_k}(\Phi_k - \Phi_{k+1}) = \nabla E[\Phi_{k+1}]$ , then

$$\|\nabla E[\Phi_{k+1}]\| \leq (L_{\mathcal{M}} + 1/\bar{\alpha})\|\Phi_{k+1} - \Phi_k\|. \quad (23)$$

Combining (22) with (23), it follows that

$$\|\nabla E[\Phi_{k+1}]\| \leq \rho_2(\|\Phi_{k+1} - \Phi_k\| + w_k\|\Phi_k - \Phi_{k-1}\|) \leq \rho_2(\|\Phi_{k+1} - \Phi_k\| + \bar{w}\|\Phi_k - \Phi_{k-1}\|), \quad (24)$$

where  $\rho_2 = L_{\mathcal{M}} + 1/\bar{\alpha} > 0$ .

**Subsequence convergence.** Since  $\{\Phi_k\} \subset \mathcal{M}$  which is compact, there exists a subsequence  $\{\Phi_{k_j}\}$  and  $\Phi^* \in \mathcal{M}$  such that

$$\lim_{j \rightarrow +\infty} \Phi_{k_j} = \Phi^*, \quad \lim_{j \rightarrow +\infty} E[\Phi_{k_j}] = E[\Phi^*] \quad \text{and} \quad \lim_{j \rightarrow +\infty} \nabla E[\Phi_{k_j}] = \nabla E[\Phi^*],$$

where the last two equalities are from the continuity of  $E$ . Moreover, (21) implies

$$\lim_{j \rightarrow +\infty} \|\Phi_{k_j} - \Phi_{k_j-1}\| = 0 \quad \text{and} \quad \lim_{j \rightarrow +\infty} \|\Phi_{k_j-1} - \Phi_{k_j-2}\| = 0.$$

Then, we know  $\nabla E[\Phi^*] = \mathbf{0}$  from (24).

**Finite length property.** Let  $\omega(\Phi_0)$  be the set of limiting points of the sequence  $\{\Phi_k\}$  starting from  $\Phi_0$ . By the boundedness of  $\{\Phi_k\}$  and the fact  $\omega(\Phi_0) = \bigcap_{q \in \mathbb{N}} \bigcup_{k \geq q} \{\Phi_k\}$ , it follows that  $\omega(\Phi_0)$  is a non-empty and compact set. Moreover, from (20), we know  $E[\Phi]$  is constant on  $\omega(\Phi_0)$ , denoted by  $E^*$ . If there exists some  $k_0$  such that  $E[\Phi_{k_0}] = E^*$ , then we have  $E[\Phi_k] = E^*$  for all  $k \geq k_0$  which is from (20). In the following proof, we assume that  $E[\Phi_k] > E^*$  for all  $k$ . Therefore,  $\forall \epsilon, \eta > 0$ , there exists some  $\ell > 0$  such that for all  $k > \ell$ , we have  $\text{dist}(\omega(\Phi_0), \Phi_k) \leq \epsilon$  and  $E^* < E[\Phi_k] < E^* + \eta$ , i.e.

$$\Phi \in \Gamma_{\eta}(\Phi^*, \epsilon) \quad \text{for all} \quad \Phi^* \in \omega(\Phi_0).$$

Applying lemma 4.4, for all  $k > \ell$  we have

$$\psi'(E[\Phi_k] - E^*)\|\nabla E[\Phi_k]\| \geq 1.$$

Form (24), it implies

$$\psi'(E[\Phi_k] - E^*) \geq \frac{1}{\rho_2(\|\Phi_k - \Phi_{k-1}\| + w_{k-1}\|\Phi_{k-1} - \Phi_{k-2}\|)}. \quad (25)$$

By the convexity of  $\psi$ , we have

$$\psi(E[\Phi_k] - E^*) - \psi(E[\Phi_{k+1}] - E^*) \geq \psi'(E[\Phi_k] - E^*)(E[\Phi_k] - E[\Phi_{k+1}]). \quad (26)$$

Define  $\Delta_{p,q} = \psi(E[\Phi_p] - E^*) - \psi(E[\Phi_q] - E^*)$  and  $C = \rho_2/\rho_1 > 0$ . Together with (25), (26) and (20), we have for all  $k > \ell$

$$\Delta_{k,k+1} \geq \frac{\|\Phi_{k+1} - \Phi_k\|_2^2}{C(\|\Phi_k - \Phi_{k-1}\| + w_{k-1}\|\Phi_{k-1} - \Phi_{k-2}\|)},$$

and therefore,

$$2\|\Phi_{k+1} - \Phi_k\| \leq \|\Phi_k - \Phi_{k-1}\| + w_{k-1}\|\Phi_{k-1} - \Phi_{k-2}\| + C\Delta_{k,k+1}, \quad (27)$$

which is from the fact that geometric inequality. For any  $k > \ell$ , summing up (27) for  $i = \ell + 1, \dots, k$ , it implies

$$\begin{aligned} 2 \sum_{i=\ell+1}^k \|\Phi_{i+1} - \Phi_i\| &\leq \sum_{i=\ell+1}^k (\|\Phi_i - \Phi_{i-1}\| + w_{i-1}\|\Phi_{i-1} - \Phi_{i-2}\|) + C \sum_{i=\ell+1}^k \Delta_{i,i+1} \\ &\leq \sum_{i=\ell+1}^k (1 + w_i)\|\Phi_{i+1} - \Phi_i\| + (1 + w_\ell)\|\Phi_\ell - \Phi_{\ell-1}\| + w_{\ell-1}\|\Phi_{\ell-1} - \Phi_{\ell-2}\| + C\Delta_{\ell+1,k+1}, \end{aligned}$$

where the last inequality is from the fact that  $\Delta_{p,q} + \Delta_{q,r} = \Delta_{p,r}$  for all  $p, q, r \in \mathbb{N}$ . Since  $\psi \geq 0$ , for any  $k > \ell$  and  $w_k \leq \bar{w}$ , we have

$$\begin{aligned} \sum_{i=\ell+1}^k (1 - \bar{w})\|\Phi_{i+1} - \Phi_i\| &\leq \sum_{i=\ell+1}^k (1 - w_i)\|\Phi_{i+1} - \Phi_i\| \\ &\leq (1 + w_\ell)\|\Phi_\ell - \Phi_{\ell-1}\| + w_{\ell-1}\|\Phi_{\ell-1} - \Phi_{\ell-2}\| + C\psi(E[\Phi_\ell] - E^*). \end{aligned}$$

This easily implies that  $\sum_{k=1}^\infty \|\Phi_{k+1} - \Phi_k\| < \infty$  and  $\lim_{k \rightarrow \infty} \Phi_k = \Phi^*$  where  $\nabla E[\Phi^*] = \mathbf{0}$ .  $\square$

## 5. Connection with gradient flows

Let  $\mathcal{L}$  be a non-positive symmetric operator, the gradient flow of energy  $E$  can be formulated as

$$\frac{\partial \phi}{\partial t} = \mathcal{L} \frac{\delta E}{\delta \phi}. \quad (28)$$

Two classical gradient flow approaches for solving the PFC model are

$$\begin{aligned} (\text{Allen-Cahn}) \quad & \frac{\partial \phi}{\partial t} = -\frac{\delta E}{\delta \phi}, \\ (\text{Cahn-Hilliard}) \quad & \frac{\partial \phi}{\partial t} = \nabla \cdot \left( M_\phi \nabla \frac{\delta E}{\delta \phi} \right), \end{aligned}$$

with appropriate boundary conditions where  $M_\phi$  is a non-positive symmetric operator dependent on  $\phi$ . Again, splitting  $E[\phi]$  into  $E[\phi] = F[\phi] + G[\phi]$ , for a given spacial discretization, the discretized energy can be formulated as

$$E_h[\Phi] = F_h[\Phi] + G_h[\Phi].$$

Typical first-order numerical approaches for solving (28) include explicit, semi-implicit and implicit schemes, i.e.

$$\frac{\Phi_{k+1} - \Phi_k}{\alpha} = \mathcal{L}_h \begin{cases} \nabla F_h[\Phi_k] + \nabla G_h[\Phi_k], & (\text{Explicit}), \\ \nabla F_h[\Phi_k] + \nabla G_h[\Phi_{k+1}], & (\text{Semi-implicit}), \\ \nabla F_h[\Phi_{k+1}] + \nabla G_h[\Phi_{k+1}], & (\text{Implicit}), \end{cases} \quad (30)$$

where  $\mathcal{L}_h$  denotes the discretization of  $\mathcal{L}$ . To build up the connection with (30), we define the generalized proximal operator.

**Definition 5.1** (Generalized proximal operator). *Let  $G$  be a proper, lower semi-continuous function and  $\mathcal{S}$  be a positive symmetric operator. The generalized proximal operator with respect to  $\mathcal{S}$  is*

$$\text{GProx}_{G,\mathcal{S}}(y) = \operatorname{argmin}_x \left\{ G(x) + \frac{1}{2} \|x - y\|_{\mathcal{S}}^2 \right\},$$

where  $\|x\|_{\mathcal{S}}^2 = \langle x, \mathcal{S}x \rangle$ .

It is noted  $\text{GProx}_{G,S}$  is non-empty and compact, see [6]. The connection between the generalized proximal operator and scheme (30) arrives the following proposition:

**Proposition 5.2.** *If  $\mathcal{L}_h$  is invertible. The schemes in (30) are equivalent to*

$$\Phi_{k+1} = \begin{cases} \text{GProx}_{0,\mathcal{I}}(\Phi_k + \alpha\mathcal{L}_h(\nabla F_h[\Phi_k] + \nabla G_h[\Phi_k])), & \text{(Explicit scheme),} \\ \text{GProx}_{\alpha G_h, -\mathcal{L}_h^{-1}}(\Phi_k + \alpha\mathcal{L}_h \nabla F_h[\Phi_k]), & \text{(Semi-implicit scheme),} \\ \text{GProx}_{\alpha(F_h+G_h), -\mathcal{L}_h^{-1}}(\Phi_k), & \text{(Implicit scheme),} \end{cases} \quad (31)$$

where  $\mathcal{I}$  is the identity operator.

*Proof.* As the proof of three schemes are similar, we only prove the semi-implicit case. It is noted that  $-\mathcal{L}_h$  is positive symmetric as  $\mathcal{L}_h$  is non-negative and invertible. Since  $\Phi_{k+1} = \text{GProx}_{\alpha G_h, -\mathcal{L}_h^{-1}}(\Phi_k + \alpha\mathcal{L}_h \nabla F_h[\Phi_k]) = \underset{\Phi}{\operatorname{argmin}} \{ \alpha G_h[\Phi] + \frac{1}{2} \|\Phi - \Phi_k - \alpha\mathcal{L}_h \nabla F_h[\Phi_k]\|_{-\mathcal{L}_h^{-1}}^2 \}$ , we have

$$0 = \alpha \nabla G_h[\Phi_k] - \mathcal{L}_h^{-1}(\Phi_{k+1} - \Phi_k - \alpha\mathcal{L}_h \nabla F_h[\Phi_k])$$

from the first order optimality condition which implies semi-implicit numerical scheme.  $\square$

**Remark 5.3.** *It is noted that  $\mathcal{L}_h = -\mathcal{I}$  in Allen-Cahn equation and  $\mathcal{L}_h = \Delta$  in Cahn-Hilliard when  $M_\phi = 1$ . Based on our analysis, it is suggested that  $\mathcal{L}_h = \Delta - \tau\mathcal{I}$  for some  $\tau > 0$  when applying the Cahn-Hilliard equation. The implicit scheme for  $\mathcal{L}_h = \Delta - \tau\mathcal{I}$  is the gradient step of the viscosity solution for certain Hamilton-Jacobi equation as pointed out in [19]. Moreover, If  $\mathcal{L}_h = (\Delta - \tau\mathcal{I})^{-1}$  for some  $\tau > 0$  in (31), the explicit scheme is the (generalized) Laplacian smoothing introduced [19].*

**Remark 5.4.** *The APG method can be formulated as*

$$\Phi_{k+1} = \text{GProx}_{\alpha G_h, \mathcal{I}}(\tilde{\Phi}_k - \alpha \nabla F_h[\tilde{\Phi}_k]), \quad \tilde{\Phi}_k = \Phi_k + w_k(\Phi_k - \Phi_{k-1}),$$

for some  $w_k \in (0, 1)$ . When the objective function is convex, the extrapolation step has been proved to accelerate convergence. Meanwhile, from the perspective of interpolation methods,  $\tilde{\Phi}_k$  can also be thought as an approximation of the implicit step. It is the Lagrange interpolation when  $w_k = 1$ .

**Remark 5.5.** *The energy dissipation is related to the objective value decreasing property of the generalized proximal operators in (31); the adaptive time stepping corresponds to the adaptive step sizes  $\alpha_k$  which can be efficiently implemented by the line search as shown in Algorithm 1.*

As the semi-implicit approach is not unconditional energy dissipation, stabilized methods have been proposed [30]. In concrete, the stabilized semi-implicit scheme contains

$$\frac{\Phi_{k+1} - \Phi_k}{\alpha} = \mathcal{L}_h(\nabla G_h[\Phi_{k+1}] + \nabla F_h[\Phi_k] + \sigma(\Phi_{k+1} - \Phi_k)).$$

for some  $\sigma > 0$ . Suppose  $\mathcal{L}_h$  is invertible and  $\mathcal{S} = -(\mathcal{I} - \sigma\alpha\mathcal{L}_h)^{-1}\mathcal{L}_h$  is positive symmetric, the above scheme is equivalent to

$$\begin{aligned} (\mathcal{I} - \sigma\alpha\mathcal{L}_h)(\Phi_{k+1} - \Phi_k) &= \mathcal{L}_h\alpha(\nabla G_h[\Phi_{k+1}] + \nabla F_h[\Phi_k]) \\ \iff \Phi_{k+1} &= \text{GProx}_{\alpha G_h, \mathcal{S}^{-1}}(\Phi_k - \alpha\mathcal{S}\nabla F_h[\Phi_k]). \end{aligned}$$

In Allen-Cahn equation,  $\mathcal{L}_h = -\mathcal{I}$ , all the required conditions are automatically satisfied. However, in Cahn-Hilliard equation, the corresponding conditions require further exploration. In general case, discovering the deep connections between the gradient flow and the proximal operators may provide new insights for both fields and we will explore it in future.

## 6. Numerical results and discussions

In this section, we present several numerical examples to illustrate the efficiency and accuracy of our method by comparing with the semi-implicit scheme (SIS). All experiments were performed on a workstation with a 3.20 GHz CPU (i7-8700, 12 processors). All code were written by MATLAB language without parallel implementation. In our experiments, the Algorithm 2 is employed to calculate the stationary states of finite dimensional PFC models, including the LB energy functional (3) with the Fourier pseudospectral discretization  $E_h$  (see Eq. (6)) for periodic crystals and the LP energy functional with the projection method discretization for quasicrystals. Let  $\Phi_s$  be the “exact” stationary state obtained numerically with a very fine mesh and  $E_s = E_h[\Phi_s]$  be its energy. Correspondingly, let  $\Phi_{s,h}$  be the numerical stationary state obtained with the mesh size  $h$  and  $E_h[\Phi_{s,h}]$  be its energy.

### 6.1. Periodic crystals

For the LB model, we use three dimensional periodic crystals of the double gyroid and the sigma phase, recently discovered both in polymer experiments and in theoretical computations [31, 15], to demonstrate the performance of our approach.

#### 6.1.1. Double gyroid

The double gyroid phase is a continuous network periodic phase. Its initial value is

$$\phi(\mathbf{r}) = \sum_{\mathbf{h} \in \Lambda_0^{DG}} \hat{\phi}(\mathbf{h}) e^{i(\mathbf{B}\mathbf{h})^T \cdot \mathbf{r}},$$

where initial lattice points set  $\Lambda_0^{DG} \subset \mathbb{Z}^3$  only on which the Fourier coefficients located are nonzero. The corresponding  $\Lambda_0^{DG}$  of the double gyroid phase is given in the Table 1. For more details, please refer to [12]. The

Table 1: The initial lattice points set  $\Lambda_0$  of the double gyroid phase.  $^o$  denotes the sign of Fourier coefficients is opposite.

$\Lambda_0^{DG}$	$(-2, 1, 1), (2, 1, 1)^o, (2, 1, -1)^o, (2, -1, 1), (1, -2, 1), (1, 2, -1), (1, 2, 1)^o, (-1, 2, 1)^o, (1, 1, -2), (1, -1, 2)^o, (-1, 1, 2), (1, 1, 2)^o$
------------------	---

double gyroid structure belongs to the cubic crystal system, therefore, the 3-order invertible matrix can be chosen as  $\mathbf{B} = (1/\sqrt{6})\mathbf{I}_3$ . Correspondingly, the computational domain in physical space is  $[0, 2\sqrt{6}\pi]^3$ . The parameters in LB model (3) are set as  $\xi = 0.1, \tau = -2.0, \gamma = 2.0$ .

The exact solution is obtained numerically by using  $256 \times 256 \times 256$  spatial discretization points, and its exact energy with such model parameters is  $E_s = -12.9429155189828$ . Table 2 presents the numerical error for the double gyroid phase. From Table 2, it is observed that the Fourier pseudospectral method is spectral accuracy. Figure 1 shows the morphology of stationary double gyroid phase.

Table 2: Accuracy of the Fourier pseudospectral discretization for the double gyroid phase in the LB model simulations. The solution with  $256 \times 256 \times 256$  is used as reference solution.

	DOF	$32^3$	$64^3$	$128^3$
Double gyroid	$\ \Phi_s - \Phi_h\ _2$	6.2770e-05	7.7191e-08	7.0668e-12
	$ E_s - E_h(\Phi_{s,h}) $	4.9949e-02	2.3984e-06	1.0658e-14

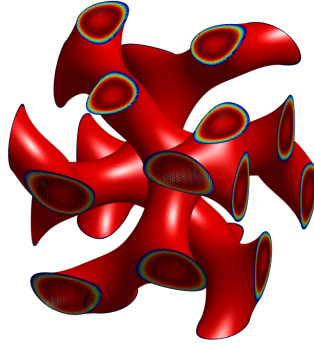


Figure 1: The stationary double gyroid phase in LB model with  $\xi = 0.1, \tau = -2.0, \gamma = 2.0$ .

In order to demonstrate the performance of our proposed method, a convergent comparison between the adaptive APG method and the SIS for the energy difference is shown in Figure 2, using  $128 \times 128 \times 128$  spacial discretization points. In the SIS, the time step  $\alpha$  is fixed, while in adaptive APG approach,  $\alpha$  can be obtained adaptively by the linear search technique, as given in Figure 3. In comparison, the fixed time step of the SIS is chosen as 0.2 to guarantee the best performance on the premise of energy dissipation. It is shown that the adaptive APG algorithm converges faster than the SIS. In particular, The adaptive APG needs 149 steps to achieve the

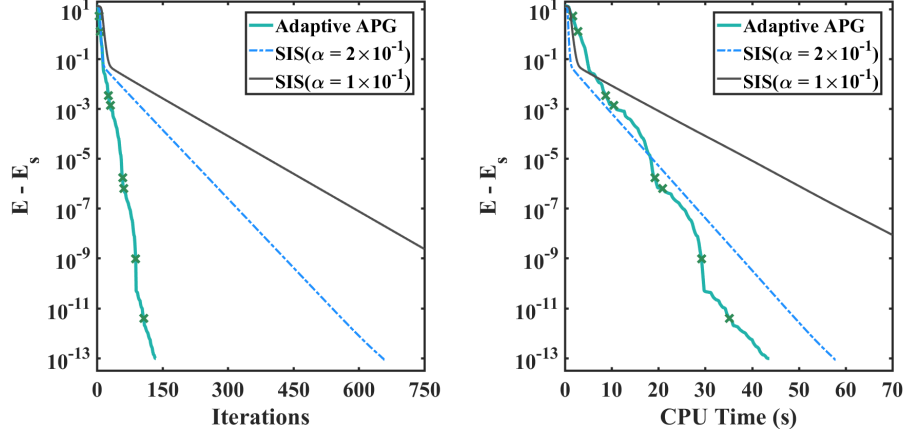


Figure 2: Comparison of convergence across different algorithms for computing the double gyroid phase. The vertical axis is the difference between the energy value in current step and the lowest attained energy value. On left, the horizontal axis is the number of iterations. On right, the horizontal axis is time taken. The  $\times$ s mark where restarts occurred.

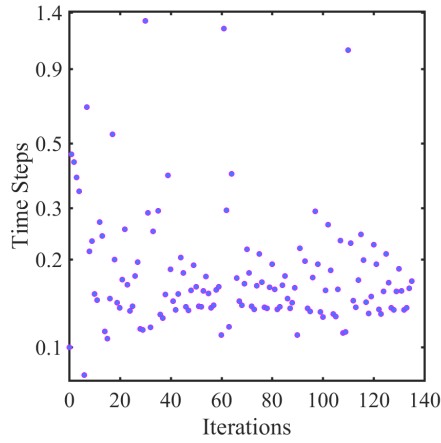


Figure 3: The adaptive time steps obtained by the adaptive APG in computing the double gyroid phase.

error level of  $10^{-13}$ , while the SIS requires 660 iterations for  $\alpha = 0.2$  and 1190 steps when  $\alpha = 0.1$ . Our proposed approach requires the linear search techniques to obtain the adaptive time step length, it may spend more time than fixed  $\alpha$  method in each iteration sometimes. However, due to the adaptive strategy, our proposed approach still costs less CPU time than the SIS.

### 6.1.2. Sigma phase

The second periodic structure considered here is the sigma phase, which is a complicated spherical packed phase recently discovered in block copolymer systems [15]. For such a pattern, we implement our algorithm on bounded computational domain  $[0, 27.7884) \times [0, 27.7884) \times [0, 14.1514)$ . The initial values are obtained from [29, 1]. When computing the sigma phase, the parameters are set as  $\xi = 1.0, \tau = 0.01, \gamma = 2.0$ . The exact solution is obtained numerically by using  $256 \times 256 \times 128$  spatial discretization points whose morphology is presented in Figure 4. Correspondingly, the convergent energy value is  $E_s = -0.93081648457086$ . As far as we know, it is the first time to find such complicated sigma phase in such a simple PFC model.

Table 3: Accuracy of the Fourier pseudospectral discretization for the sigma phase in the LB model simulations. The solution with  $256 \times 256 \times 128$  is used as reference solution.

	DOF	$128 \times 128 \times 64$	$160 \times 160 \times 80$	$200 \times 200 \times 100$
Sigma	$\ \Phi_s - \Phi_h\ _2$	2.2710e-06	7.1800e-11	7.3107e-12
	$ E_s - E_h(\Phi_{s,h}) $	4.2930e-03	2.3648e-14	2.3315e-15

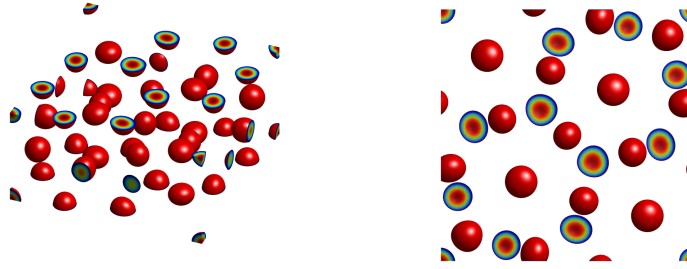


Figure 4: The stationary sigma phase from two views in LB model with  $\xi = 1.0, \tau = 0.01, \gamma = 2.0$ .

Figure 5 gives the convergence between the adaptive APG method and the SIS for the energy difference. Again, on the premise of energy dissipation, the time step  $\alpha$  in the SIS is chosen as 0.4 to demonstrate its best performance. Our proposed algorithm still can obtain adaptive time step by the linear search technique, as demonstrated in Figure 6. Obviously, from Figure 5, the adaptive APG algorithm is more efficient than the SIS. In concrete, the adaptive APG approach reaches an error about  $10^{-13}$  in 247.3 secs with 174 iterations. The SIS with fixed step length  $\alpha = 0.4$  (0.3) requires 851 (1086) iterations and 370.3 (474.5) secs to achieve the same accuracy.

### 6.2. Quasicrystals

For the LP free energy, we take the two dimensional dodecagonal quasicrystal as an example to examine the performance of our proposed approach. For dodecagonal quasicrystals, two length scales  $q_1$  and  $q_2$  equal to 1 and  $2 \cos(\pi/12)$ , respectively. Two dimensional dodecagonal quasicrystals can be embedded into four dimensional periodic structures, therefore, the projection method is required to implement in four dimension. The 4-order invertible matrix  $\mathbf{B}$  associated with to four dimensional periodic structure is chosen as  $\mathbf{I}_4$ . The corresponding computational domain in real space is  $[0, 2\pi)^4$ . The projection matrix  $\mathcal{P}$  in Eq. (8) of the dodecagonal quasicrystals is

$$\mathcal{P} = \begin{pmatrix} 1 & \cos(\pi/6) & \cos(\pi/3) & 0 \\ 0 & \sin(\pi/6) & \sin(\pi/3) & 1 \end{pmatrix}.$$

The initial solution is

$$\phi(\mathbf{r}) = \sum_{\mathbf{h} \in \Lambda_0^{QC}} \hat{\phi}(\mathbf{h}) e^{i[(\mathcal{P} \cdot \mathbf{B} \mathbf{h})^T \cdot \mathbf{r}]}, \quad \mathbf{r} \in \mathbb{R}^2,$$

where initial lattice points set  $\Lambda_0^{QC} \subset \mathbb{Z}^4$  on which the Fourier coefficients  $\hat{\phi}(\mathbf{h})$  located are nonzero of dodecagonal quasicrystal is given in the Table 4.

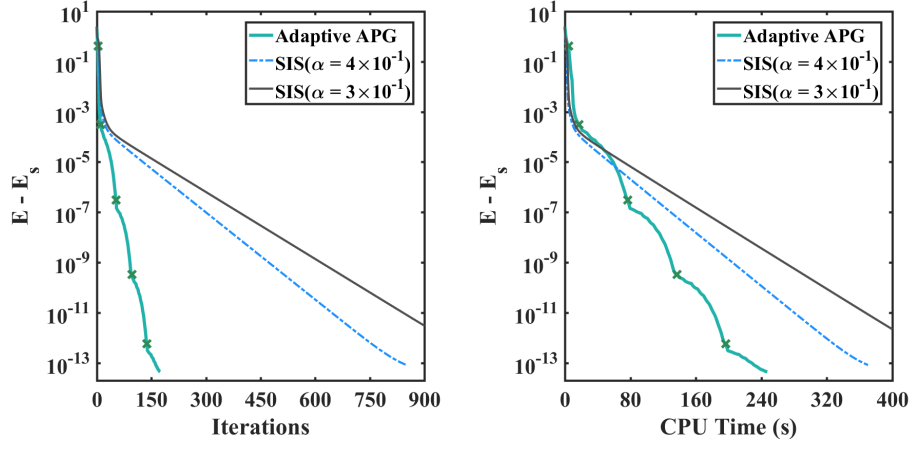


Figure 5: Comparison of convergence across different algorithms for computing the sigma phase. The vertical axis is the difference between the energy value in current step and the lowest attained energy value. On left, the horizontal axis is the number of iterations. On right, the horizontal axis is time taken. The x's mark where restarts occurred.

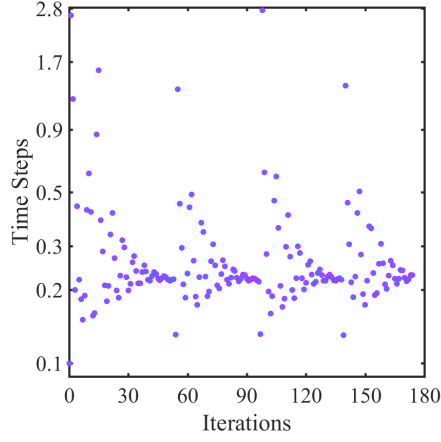


Figure 6: The adaptive time steps obtained by the adaptive APG in computing the sigma phase.

Table 4: The initial lattice points  $\Lambda_0^{QC}$  of dodecagonal quasicrystals.

$\mathbf{h} \in \Lambda_0^{QC}$	$(0\ 1\ 0\ -1)\ (0\ -1\ 0\ 1)\ (1\ 0\ 0\ 0)\ (-1\ 0\ 0\ 0)\ (0\ 1\ 0\ 0)\ (0\ -1\ 0\ 0)$ $(0\ 0\ 1\ 0)\ (0\ 0\ -1\ 0)\ (0\ 0\ 0\ 1)\ (0\ 0\ 0\ -1)\ (-1\ 0\ 1\ 0)\ (1\ 0\ -1\ 0)$ $(1\ 1\ 0\ -1)\ (-1\ -1\ 0\ 1)\ (1\ 1\ 0\ 0)\ (-1\ -1\ 0\ 0)\ (0\ 1\ 1\ 0)\ (0\ -1\ -1\ 0)$ $(0\ 0\ 1\ 1)\ (0\ 0\ -1\ -1)\ (-1\ 0\ 1\ 1)\ (1\ 0\ -1\ -1)\ (-1\ -1\ 1\ 1)\ (1\ 1\ -1\ -1)$
---------------------------------	--

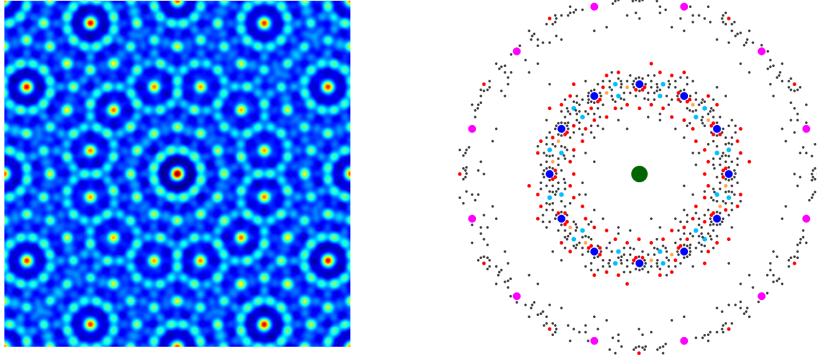


Figure 7: The stationary dodecagonal quasicrystal in LP model with  $c = 1.5, \varepsilon = -6.0, \kappa = 0.3$ . The left plot is the physical morphology. The right subfigure is the Fourier spectral points whose coefficient intensity is larger than 0.01.

When computing the dodecagonal quasicrystal, the parameters in LP model are set as  $c = 1.5, \varepsilon = -6.0, \kappa = 0.3$ , and  $38^4$  spatial discretization points are used. The convergent stationary quasicrystal including its morphology and Fourier spectrum is given in Figure 7. The finally convergent energy value obtained by the adaptive APG approach is  $E_s = -5.76164741513328$ . The iterative behavior of our proposed method and the SIS with different fixed time steps,  $\alpha = 0.1, 0.05, 0.005$ , is found in Figure 8. The adaptive time steps of our proposed approach is given in Figure 9. In the SIS, the energy difference decreases to the error level of about  $10^{-6.8}$ , then increases for all given time step  $\alpha$ . However, the adaptive APG algorithm is always energy dissipation as Theorem 4.5 predicted. These results demonstrates that the adaptive APG approach is more robust for finding the stationary states.

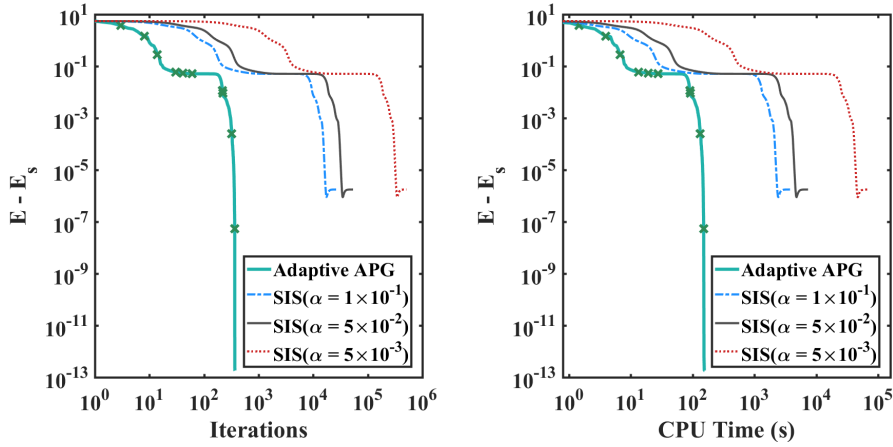


Figure 8: Comparison of convergence across different algorithms for computing the dodecagonal phase. The vertical axis is the difference between the energy value in current step and the lowest attained energy value. On left, the horizontal axis is the number of iterations. On right, the horizontal axis is time taken. The  $\times$ s mark where restarts occurred.

## 7. Conclusion

In this paper, a fast, efficient, and robust computational approach has been proposed to find the stationary states of PFC models. The adaptive APG method is obtained through a combination of the SIS and the restart APG approach. Instead of formulating the energy minimization as a gradient flow, we applied the adaptive APG method directly on the discretized energy with proved local convergence. Extensive results in computing periodic crystals and quasicrystals have shown its advantage in terms of computation efficiency without loss of the accuracy. Moreover, the preliminary connections between the numerical schemes in solving gradient flow and the generalized proximal operator are present in this work and motivate us to continue finding its deep relationship in future.

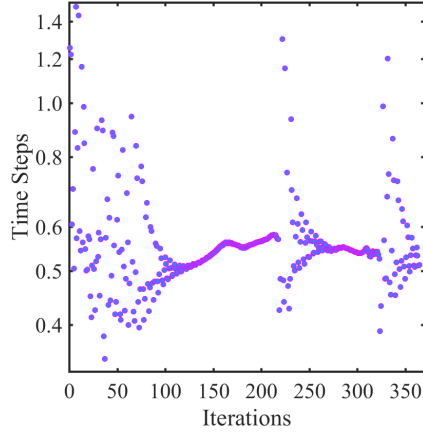


Figure 9: The adaptive time steps obtained by the adaptive APG in computing the dodecagonal phase.

### Acknowledgements

This work is supported by the National Natural Science Foundation of China (11771368) and the Project of Scientific Research Fund of Hunan Provincial Science and Technology Department (2018WK4006). KJ is partially supported by the Hunan Science Foundation of China (2018JJ2376), the Youth Project Hunan Provincial Education Department of China (Grant No. 16B257),

## References

- [1] A. ARORA, J. QIN, D. C. MORSE, K. T. DELANEY, G. H. FREDRICKSON, F. S. BATES, AND K. D. DORFMAN, *Broadly accessible self-consistent field theory for block polymer materials discovery*, *Macromolecules*, 49 (2016), pp. 4675–4690.
- [2] C. BAO, G. BARBASTATHIS, H. JI, Z. SHEN, AND Z. ZHANG, *Coherence retrieval using trace regularization*, *SIAM J. Imaging Sci.*, 11 (2018), pp. 679–706.
- [3] C. BAO, B. DONG, L. HOU, Z. SHEN, X. ZHANG, AND X. ZHANG, *Image restoration by minimizing zero norm of wavelet frame coefficients*, *Inverse Probl.*, 32 (2016), p. 115004.
- [4] J. BARZILAI AND J. M. BORWEIN, *Two-point step size gradient methods*, *IMA J. Numer. Anal.*, 8 (1988), pp. 141–148.
- [5] A. BECK AND M. TEOULLE, *A fast iterative shrinkage-thresholding algorithm for linear inverse problems*, *SIAM J. Imaging sci.*, 2 (2009), pp. 183–202.
- [6] J. BOLTE, S. SABACH, AND M. TEOULLE, *Proximal alternating linearized minimization for nonconvex and nonsmooth problems*, *Math Program.*, 146 (2014), pp. 459–494.
- [7] S. A. BRAZOVSKII, *Phase transition of an isotropic system to a nonuniform state*, *Sov. Phys. JETP*, 41 (1975), p. 85.
- [8] L. CHEN, *Phase-field models for microstructure evolution*, *Annu. Rev. Mater. Res.*, 32 (2002), pp. 113–140.
- [9] T. DOTERA, T. OSHIRO, AND P. ZIHERL, *Mosaic two-lengthscale quasicrystals*, *Nature*, 506 (2014), p. 208.
- [10] H. HILLER, *The crystallographic restriction in higher dimensions*, *Acta Cryst. Sect. A*, 41 (1985), pp. 541–544.
- [11] K. JIANG, J. TONG, P. ZHANG, AND A.-C. SHI, *Stability of two-dimensional soft quasicrystals in systems with two length scales*, *Phys. Rev. E*, 92 (2015), p. 042159.
- [12] K. JIANG, C. WANG, Y. HUANG, AND P. ZHANG, *Discovery of new metastable patterns in diblock copolymers*, *Commun. Comput. Phys.*, 14 (2013), pp. 443–460.
- [13] K. JIANG AND P. ZHANG, *Numerical methods for quasicrystals*, *J. Comput. Phys.*, 256 (2014), pp. 428–440.
- [14] Y. KATZNELSON, *An introduction to harmonic analysis*, 2nd ed., Dover, 1976.
- [15] S. LEE, M. J. BLUEMLE, AND F. S. BATES, *Discovery of a frank-kasper  $\sigma$  phase in sphere-forming block copolymer melts*, *Science*, 330 (2010), p. 349.
- [16] R. LIFSHITZ AND H. DIAMANT, *Soft quasicrystals—Why are they stable?*, *Philos. Mag.*, 87 (2007), pp. 3021–3030.
- [17] R. LIFSHITZ AND D. M. PETRICH, *Theoretical model for Faraday waves with multiple-frequency forcing*, *Phys. Rev. Lett.*, 79 (1997), pp. 1261–1264.
- [18] X. LIU, Z. WEN, X. WANG, M. ULBRICH, AND Y. YUAN, *On the analysis of the discretized Kohn–Sham density functional theory*, *SIAM J. Numer. Anal.*, 53 (2015), pp. 1758–1785.
- [19] S. OSHER, B. WANG, P. YIN, X. LUO, M. PHAM, AND A. LIN, *Laplacian smoothing gradient descent*, *arXiv preprint arXiv:1806.06317*, (2018).
- [20] B. O’DONOGHUE AND E. CANDÈS, *Adaptive restart for accelerated gradient schemes*, *Found. Comput. Math.*, 15 (2015), pp. 715–732.
- [21] N. PROVATAS AND K. ELDER, *Phase-field methods in materials science and engineering*, Wiley-VCH, 2010.
- [22] J. SHEN, J. XU, AND J. YANG, *The scalar auxiliary variable (SAV) approach for gradient flows*, *J. Comput. Phys.*, 353 (2018), pp. 407–416.
- [23] A.-C. SHI, J. NOOLANDI, AND R. C. DESAI, *Theory of anisotropic fluctuations in ordered block copolymer phases*, *Macromolecules*, 29 (1996), pp. 6487–6504.
- [24] W. SU, S. BOYD, AND E. CANDÈS, *A differential equation for modeling Nesterovs accelerated gradient method: Theory and insights*, *Adv. Neural Inf. Process. Syst.*, 2014, pp. 2510–2518.
- [25] J. SWIFT AND P. C. HOHENBERG, *Hydrodynamic fluctuations at the convective instability*, *Phys. Rev. A*, 15 (1977), p. 319.
- [26] P. TSENG, *On accelerated proximal gradient methods for convex-concave optimization*, submitted to *SIAM J. Optim.*, 2 (2008), p. 3.
- [27] M. ULBRICH, Z. WEN, C. YANG, D. KLOCKNER, AND Z. LU, *A proximal gradient method for ensemble density functional theory*, *SIAM J. Sci. Comput.*, 37 (2015), pp. A1975–A2002.
- [28] X. WU, Z. WEN, AND W. BAO, *A regularized Newton method for computing ground states of Bose–Einstein condensates*, *J. Sci. Comput.*, 73 (2017), pp. 303–329.
- [29] N. XIE, W. LI, F. QIU, AND A.-C. SHI,  *$\sigma$  phase formed in conformationally asymmetric ab-type block copolymers*, *ACS Macro Lett.*, 3 (2014), pp. 906–910.
- [30] C. XU AND T. TANG, *Stability analysis of large time-stepping methods for epitaxial growth models*, *SIAM J. Numer. Anal.*, 44 (2006), pp. 1759–1779.
- [31] P. ZHANG AND X. ZHANG, *An efficient numerical method of Landau–Brazovskii model*, *J. Comput. Phys.*, 227 (2008), pp. 5859–5870.